

Journal Pre-proofs

Research Article

Structural analysis of the human C5a-C5aR1 complex using cryo-electron microscopy

Tingting Yang, Jian Li, Xinyu Cheng, Qiuyuan Lu, Zara Farooq, Ying Fu, Sijia Lv, Weiwei Nan, Boming Yu, Jingjing Duan, Yuting Zhang, Yang Fu, Haihai Jiang, Peter J McCormick, Yanyan Li, Jin Zhang

PII: S1047-8477(24)00057-1
DOI: <https://doi.org/10.1016/j.jsb.2024.108117>
Reference: YJSBI 108117

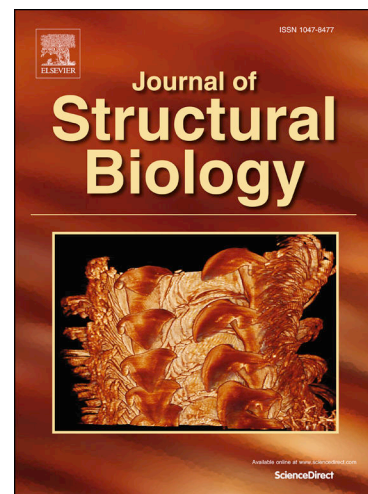
To appear in: *Journal of Structural Biology*

Received Date: 6 May 2024
Revised Date: 7 August 2024
Accepted Date: 14 August 2024

Please cite this article as: Yang, T., Li, J., Cheng, X., Lu, Q., Farooq, Z., Fu, Y., Lv, S., Nan, W., Yu, B., Duan, J., Zhang, Y., Fu, Y., Jiang, H., McCormick, P.J., Li, Y., Zhang, J., Structural analysis of the human C5a-C5aR1 complex using cryo-electron microscopy, *Journal of Structural Biology* (2024), doi: <https://doi.org/10.1016/j.jsb.2024.108117>

This is a PDF file of an article that has undergone enhancements after acceptance, such as the addition of a cover page and metadata, and formatting for readability, but it is not yet the definitive version of record. This version will undergo additional copyediting, typesetting and review before it is published in its final form, but we are providing this version to give early visibility of the article. Please note that, during the production process, errors may be discovered which could affect the content, and all legal disclaimers that apply to the journal pertain.

© 2024 Published by Elsevier Inc.



Structural Analysis of the human C5a-C5aR1 Complex using Cryo-Electron Microscopy

Tingting Yang^{a,#}, Jian Li^{b,c,#}, Xinyu Cheng^{a,#}, Qiuyuan Lu^{d,e,#}, Zara Farooq^{f,#}, Ying Fu^a, Sijia Lv^a, Weiwei Nan^a, Boming Yu^g, Jingjing Duan^g, Yuting Zhang^h, Yang Fuⁱ, Haihai Jiang^{a,*}, Peter J McCormick^{f,j,*}, Yanyan Li^{d,e,*}, Jin Zhang^{a,*}

^a The MOE Basic Research and Innovation Center for the Targeted Therapeutics of Solid Tumors, School of Basic Medical Sciences, Jiangxi Medical College, Nanchang University, Nanchang, China; The Second Affiliated Hospital, Jiangxi Medical College, Nanchang University, Nanchang, China..

^b College of Pharmaceutical Sciences, Gannan Medical University, Ganzhou, 341000, Jiangxi, PR, China.

^c Laboratory of Prevention and treatment of cardiovascular and cerebrovascular diseases, Ministry of Education, Gannan Medical University, Ganzhou 341000, PR China

^d Institute for Biological Electron Microscopy, Southern University of Science and Technology, Shenzhen, Guangdong, 518055, China

^e Department of Chemical Biology, School of Life Southern University of Science and Technology, Shenzhen, Guangdong, 518055, China

^f William Harvey Research Institute, Bart's and the London School of Medicine and Dentistry, Queen Mary University of London, London, UK

^g Human Aging Research Institute (HARI), School of Life Sciences, Nanchang University, Nanchang, Jiangxi, 330031, China

^h Shenzhen Crystal Biopharmaceutical Co., Ltd, Shenzhen, Guangdong, 518118, China

ⁱ School of Medicine, Southern University of Science and Technology, Shenzhen, Guangdong, China 518055

^j Department of Pharmacology and Therapeutics, University of Liverpool, Liverpool, UK, L69 3GE

These authors contributed equally to this work.

* Correspondence: zhangxiaokong@hotmail.com (Jin Zhang); liyy6@sustech.edu.cn (Yanyan Li); P.mccormick@qmul.ac.uk (Peter J McCormick); haihaijiang2020@ncu.edu.cn (Haihai Jiang).

Abstract

The complement system is a complex network of proteins that plays a crucial role in the innate immune response. One important component of this system is the C5a-C5aR1 complex, which is critical in the recruitment and activation of immune cells. In-depth investigation of the activation mechanism as well as biased signaling of the C5a-C5aR1 system will facilitate the elucidation of C5a-mediated pathophysiology. In this study, we determined the structure of C5a-C5aR1-Gi complex at a high resolution of 3 Å using cryo-electron microscopy (Cryo-EM). Our results revealed the binding site of C5a, which consists of a polar recognition region on the extracellular side and an amphipathic pocket within the transmembrane domain. Furthermore, we found that C5a binding induces conformational changes of C5aR1, which subsequently leads to the activation of G protein signaling pathways. Notably, a key residue (M265) located on transmembrane helix 6 (TM6) was identified to play a crucial role in regulating the recruitment of β -arrestin driven by C5a. This study provides more information about the structure and function of the human C5a-C5aR1 complex, which is essential for the proper functioning of the complement system. The findings of this study can also provide a foundation for the design of new pharmaceuticals targeting this receptor with bias or specificity.

Keywords: G protein-coupled receptor (GPCR), C5aR1, structure, complement system, cryo-electron microscopy

Introduction

The tremendous success of immunotherapies in oncology has sparked renewed interest in identification of novel ways to modulate the immune system to enhance immune based anti-tumor approaches, with checkpoint inhibitors being an excellent example. One rich source for drug targets are the super family of G-protein coupled receptors (GPCRs) (Hauser et al., 2017; Hauser et al., 2018). A recent example of using GPCRs to improve immunotherapy is to target the adenosine A2a receptor (Solino et al., 2022; Sun et al., 2022; Vigano et al., 2019). More recently, it has been appreciated that altering innate immunity via the complement system could be an effective approach towards improving immunotherapy (Talaat et al., 2022). The complement system is a crucial component of host defense and includes antibody recognition complexes or pattern recognition receptors. It also contains convertases, which are enzymes responsible for producing a range of immune-activating pro-inflammatory peptides known as anaphylatoxins, among others (Merle et al., 2015). Anaphylatoxins bind in part to two GPCRs, C3aR and C5aR1 (CD88) (Ajona et al., 2019; Klos et al., 2009; Schanzenbacher et al., 2022). One of these peptides, C5a, is produced from the complement component C5 by the enzyme C5 convertase, which cleaves C5 into C5a and C5b (Horiuchi & Tsukamoto, 2016; Quadros & Cunha, 2016). C5a can serve as a chemoattractant for immune cells to the site of infection or injury, and it also stimulates the release of other inflammatory mediators (An et al., 2014; Darling et al., 2015; Li & Liu, 2021; Sadik et al., 2018; Zhang et al., 2021). The targeting of the C5a peptide via the inhibitors eculizumab and coversin among others have been used effectively to block binding while more recently there have been biologics developed to bind either peptide or receptor (Ardissino et al., 2022; Ricklin & Lambris, 2007; Woodruff et al., 2011). C5a specifically binds to the GPCR C5aR1, while C3a selectively interacts with its cognate receptor C3aR. C5aR1 is found on a variety of cells, including neutrophils, monocytes, macrophages, and mast cells, and it plays an important role in the inflammatory response (Shi et al., 2021). In T-cells these receptors modulate cell survival via mTOR activity and ROS production (West et al., 2018). In antigen-presenting cells they help drive secretion of key cytokines and maintain a balance of

Th1, Th2 and Th17 T-cells vs Tregs (Arbore et al., 2016; Mehta et al., 2015). Thus, C5a-C5aR1 modulation represents an attractive drug target.

Drugs that target C5aR1 are being developed as a potential treatment for a variety of inflammatory and immune-mediated diseases, such as rheumatoid arthritis, lupus (Anliker-Ort et al., 2020; Tampe et al., 2022), and sepsis (Fattahi et al., 2020; Sommerfeld et al., 2021). These drugs work by inhibiting the activity of C5aR1, which can help to reduce the inflammation and immune response that contribute to these conditions. Some examples of drugs that target C5aR1 include avacopan and CCX168. Avacopan, a small molecule investigational drug, targets the complement component 5a receptor, with a primary focus on C5aR1. It is currently being developed as a potential treatment option for various inflammatory and immune-mediated diseases such as ANCA-associated vasculitis (AAV) and hidradenitis suppurativa (HS) (Jayne et al., 2021; Lee, 2022; Marceau & Petitclerc, 2022). The mechanism of action of avacopan is through selective blocking of the activity of C5aR1, which is believed to have a significant role in the inflammation and immune response that contribute to the pathogenesis of these diseases. Through inhibiting the activity of C5aR1, avacopan may potentially reduce inflammation and tissue damage, thereby improving the symptoms of these diseases (Bruchfeld et al., 2022; Gabilan et al., 2022; Harigai & Takada, 2022). The U.S. Food and Drug Administration (FDA) granted marketing approval to Tavneos (avacopan) on October 8, 2021, marking a significant milestone as the first FDA-approved drug for anti-neutrophil cytoplasmic antibody-associated vasculitis in the past decade. Moreover, this achievement represents a groundbreaking achievement as the inaugural oral complement 5a receptor inhibitor sanctioned by the FDA.

Crystal structures of C5aR1 bound to an antagonist and allosteric modulators were reported by Robertson et al. and Liu et al., revealing the receptor's homomeric dimeric state (Liu et al., 2018; Robertson et al., 2018). C5aR1 has been found to couple to both Gi/o alpha subunits and β -arrestin upon activation (Buhl et al., 1994; Perianayagam et al., 2002). Molecular basis for the activation and signaling bias of C5aR1 has been described recently (Feng et al., 2023; Wang et al., 2023; Yadav et al., 2023). Here we also report the cryo-EM structure of C5a bound to C5aR1-Gi. Structural analysis of

C5a-C5aR-Gi complex coupled with functional characterization provides more information about ligand binding and signaling features of C5aR1.

Journal Pre-proofs

Results

Overall structure

We co-expressed C5a, C5aR1, heterotrimeric Gi protein, and scFv16 in insect cells using the LgBit-HiBit system and purified the complex by Ni-NTA affinity chromatography and size exclusion chromatography (Duan et al., 2020; Shao et al., 2022). HiBiT tag is extremely small (only 11 amino acids) and exhibits high affinity to LgBiT tag, facilitating the formation of GPCR complexes without affecting protein function. The structure of the purified complex was determined by single-particle cryo-EM analysis with an overall resolution of 3.0 Å (PDB ID 8IN5) (Figure 1, Figure S1, and “Methods”). Three structures of C5a-C5aR1-G complex were reported previously (Feng et al., 2023; Wang et al., 2023). Superimposition of our C5a-C5aR1-G structure and previously reported structures revealed highly similar conformation (Figure S2), with the root mean square deviation (RMSD) values ranging from 0.894 to 1.300 Å. In our C5a-C5aR1-Gi structure, the density of C5a ligand was clearly observed in the extracellular part (Figure 1A and 1B). Based on this structure, an analysis of the modes of receptor activation and endogenous agonist binding was conducted. Using transfected HEK293 cells we measured the inhibition of forskolin induced cAMP production after stimulation of C5aR1 using the real-time cAMP pGlo biosensor (Figure 1C). In line with published experiments (Paczkowski et al., 1999), we found an EC_{50} of 0.1648 nM.

The maps revealed well-defined densities for C5a in the extracellular domain and the orthosteric pocket (Figure S3). However, it was noted that the clear densities for the initial 26 amino acids (1-26 aa) and the last 46 amino acids (304-350 aa) of the C-terminus of C5aR1 were absent, suggesting a flexible conformation for these regions (Figure 1A and 1B). Additionally, the alpha-helical domain of Gi displayed poor resolution, a characteristic commonly observed in cryo-EM structures of G protein-coupled receptor (GPCR)-G protein complexes.

C5a binding site

C5a is a small protein that is produced as a part of the complement system, which is a

key component of the innate immune system. The actions of C5a are mediated by its binding to a specific receptor, C5aR1. Dysregulation of C5a and its receptor has been associated with various pathological conditions such as sepsis, atherosclerosis, and rheumatoid arthritis (Helske et al., 2008; Matsumoto et al., 2005). Our structure revealed that the size and shape of C5a are well-suited for the receptor's binding region. All 74 amino acids of C5a were meticulously resolved, thereby facilitating a remarkable conformational fit within the observed density. The structure of C5a exhibits a four-helix ($\alpha 1$ - $\alpha 4$) bundle architecture, with the C-terminus adopting a hook-like conformation that deeply inserts into the orthosteric binding site (Figure 2A, S3 and S4). Notably, our cryo-EM structure of C5a differs significantly from previously reported crystal structure of C5a (Schatz-Jakobsen et al., 2014), as the $\alpha 1$ helix is observed to be parallel to the $\alpha 2$ helix upon binding to the receptor and interacting with the N-terminal domain of C5aR1 (Figure 2A). Furthermore, the C-terminal of C5a, which is a small α helix in crystal structures, adopts a hook-like loop in the C5a-C5aR1 complex and extensively interacts with residues within the orthosteric binding pocket (Figure 2C). We achieved a resolution of 4 angstroms in the resolution of C5a. In contrast to the four low-resolution helices, the C-terminal hooked structure of C5a displays a higher resolution. This improvement is likely due to its interaction with C5aR1, which contributes to the stabilization of this specific region in the structure. This binding configuration adopts a two-site model, which is characterized by a polar recognition region on the extracellular side and an amphipathic pocket within the transmembrane domain, a feature also observed in chemokine receptors. In Site 1, the structure of C5a provides an extensive interaction network with the N-terminus and extracellular loop 2 (ECL2). The D24 residue of the $\alpha 2$ helix in C5a forms a hydrogen bond with D27^{N-term} of C5aR1, as well as a salt bridge with K28^{N-term} of C5aR1 (Figure 2B). In addition, the side chain of D191^{ECL2} establishes a hydrogen-bond interaction with S66 of C5a, which, along with the extensive hydrophobic interactions established between F182^{ECL2} and P183^{ECL2} and nearby C5a residues (namely, Q3, I6, Y23, and C27), contribute to the overall interactions between these molecules (Figure 2B). This binding mode of C5a at the N-terminus is consistent with

previous functional studies and mutational analysis, which have revealed that the N-terminus and ECL2 bind C5a and that the mutation of D27, K28 and other residues to alanine reduces the responses elicited by C5a.

The orthosteric binding pocket of C5aR1, composed of TM2, TM3, TM5-7, and C5aR1, serves as the location of Site 2 in the C5a binding site (Figure 2C). This site is stabilized by a network of polar interactions, including salt bridges and hydrogen bonds, established by specific residues such as R175, D191, E199, T261, D282, and S283 (Figure S5). Mutagenesis studies have revealed the pivotal role played by a few key regions in the activation of G protein by C5a, including the amino acids around F267^{6,60}, M265^{6,58}, K279^{7,32} and E269^{ECL3} with particular emphasis on Y258^{6,51} and D282^{7,35}. Notably, mutation of both the latter two residues blocked G-protein driven inhibition of cAMP (Figure 1C and 2C). These findings are consistent with previous studies and further reinforce the significance of the C-terminal loop in both the activity of C5a and its interaction with its receptor. The C5a binding site of C5aR1 is a well-defined pocket located in the extracellular N-terminal domain and transmembrane domain of the receptor, which serves as the binding of C5a. In a previous study, the agonist BM213 and antagonist C089 of C5aR1 were found to bind at the same site, characterized by a hook-like structure similar to that of C5a, facilitating insertion into the binding pocket of C5aR1 (Figure 2D) (Feng et al., 2023). Upon binding to this site, conformational changes occur in the receptor, triggering G protein signaling activation and downstream inflammatory responses.

Receptor activation

To examine the activation mechanism of C5aR1, we compared the previously reported C5aR1 structure in antagonist (PMX53)-bound inactive state (PDB ID 6C1Q) (Liu et al., 2018; Wang et al., 2023). Compared with C5aR1 in inactive state, TM6 in our structure has undergone an outward displacement of approximately 8.0 Å, while TM7 has shifted approximately 6.0 Å towards TM5 (Figure 3A). These structural changes are typical of G protein-coupled receptors and allow for the activation of downstream signaling pathways (Figure 3A and 3B). At the ligand-binding site, PMX53 is a small molecule inhibitor of C5aR1 that binds to the receptor in a similar way as the natural

ligand C5a, but with higher affinity and selectivity (Köhl, 2006). From the figure, it is evident that PMX53 shares a similar hook-shaped domain with C5a and occupies the binding pocket of C5aR1. However, notably, the C-terminal hook-shaped structure of C5a extends more profoundly (Figure S4B). The binding of the agonist to the C5aR1 structure results in a significant conformational change, specifically, an inward movement of the extracellular side of TM7 by 1.5 Å (Figure 3A). This movement is accompanied by the shift of residues A289^{7.42} and N292^{7.45} towards TM6, which subsequently pushes the rotamers of W255^{6.48} inward (Figure 3A). It is noteworthy that the F^{6.47}W^{6.48}xP^{6.50} motif, of which W255^{6.48} is a part, represents a conserved mechanical activation switch within class A G protein-coupled receptors. This structural information can contribute to comprehending the mechanism of C5aR1 activation and its involvement in the inflammatory response.

The movement of F^{6.47}W^{6.48}xP^{6.50} motif upon agonist binding causes a structural rearrangement in the P^{5.50}I^{3.40}F^{6.44} motif, which is also essential for receptor activation. This rearrangement is characterized by the inward rotations of the W255^{6.48} rotamer and N292^{7.45}, resulting in the flipping of the F251^{6.44} towards TM5 and the significant displacement of F211^{5.51} proximal to the motif (Figure 3A). This movement is also responsible for the significant outward motion of TM6, subsequently leading to structural rearrangements in the conserved N^{7.49}P^{7.50}xxY^{7.53} and D^{3.49}R^{3.50}F^{3.51} (also (D/E)RY motif in other GPCRs) motifs, which are crucial for maintaining receptor stability and modulating receptor signaling. In the N^{7.49}P^{7.50}xxY^{7.53} motif, Y300^{7.53} undergoes a significant displacement towards the intracellular core and establishes interactions with L127^{3.43}, I130^{3.46}, and R134^{3.50}, resulting in the inward movement of TM7 (Figure 3B). In addition to G-protein driven signaling we also examined arrestin 3 (β-arrestin 2) recruitment. We found WT receptor was able to recruit β-arrestin 2 in line with published data (Pandey et al., 2019). Intriguingly, we found that mutation of the methionine at M265^{6.58} completely abrogated β-arrestin 2 recruitment, despite this same mutant showing no major change in G-protein driven signaling (Figure 1C, 3C, 3D and 5). In addition to forming a hydrogen bond with K68 on C5a, M265 in C5aR1 also engages in hydrophobic interactions with M70 on C5a, as well as van der Waals forces

with R74. M265A mutation may disrupt the interaction network of M265, leading to a reduction in downstream β -arrestin recruitment. We then screened some of the surrounding residues within that interface and found numerous key contacts in that region that appear important for arrestin recruitment. As seen with cAMP production Y258^{6.51} and D282^{7.35} also showed no arrestin recruitment. However, in addition to M265^{6.58}, L277A and E269^{ECL3} both showed impaired arrestin recruitment despite showing activity in the cAMP assays (Figure 1C). These data support for the notion that distinct amino acid interactions drive cAMP production vs arrestin recruitment, thereby suggesting the potential development of ligands with conformational bias. In summary, the binding of C5a to C5aR1 leads to a conformational change in the receptor that brings the transmembrane helices closer together and activates G protein signaling with differential residues responsible for arrestin recruitment.

C5aR1-Gi complex interface

Previous structural studies have shown that the binding manner of G α i to the receptor is variable, with different rotations of G α i relative to the receptor. Several different states, including both canonical and non-canonical, have been identified in the NTSR1 or GHSR-Gi complex, with a rotation of 45 degrees being observed in the G-protein relative to the receptor (Liu et al., 2021; Maharana & Shukla, 2021). The G α i protein in the structure of C5aR1 is observed to be in a canonical state. Similar to the majority class A GPCRs, ICL2 of C5aR1 exhibits a short alpha-helix when in the active state. The residue at position ICL2 has been found to play a crucial role in G-protein activation by binding within the hydrophobic pocket of G α i. The interface between the receptor and the G α i protein is primarily constituted by the cytoplasmic termini of TM3, TM6, TM7, ICL2 and ICL3 (Figure 4A and 4B) (Huang & Tao, 2014; Yang & Tao, 2020). The key residues in C5aR1, namely R232, T240, R134, N71, N146, and Q145, establish hydrogen bonds with D341, F354, C351, D350, N146 and D193 in G α i respectively to form a stable complex. This interface is largely conserved between the C5a and other Class A GPCR complex structures. We compared the structures of other resolved C5aR1-G α o protein complexes (PDB ID 8IA2 and 8HPT) and found minimal differences in the binding positions and interaction interfaces between G α i and G α o

with the receptor. Their structures largely overlap. Notably, the interaction between specific amino acid residues in G α i and the receptor, as well as the positioning of a short alpha-helical turn in the receptor into a hydrophobic groove formed by specific regions of G α i, are crucial for the overall interaction. Furthermore, the engagement between the receptor and G α i is further enhanced by the interaction of specific amino acid residues in the receptor with specific residues in G α i.

Discussion

Here, we present the cryo-EM structure of the human C5aR1-Gi complex bound to its native agonist, C5a. This structure reveals essential contacts between ligand and receptor, including at least one (M265) that directs arrestin recruitment. The ligand interaction is reminiscent of chemokine interactions, with a two-site binding mechanism. When C5a binds to the receptor C5aR1, it induces an outward movement of TM6 by 8 Å and a 6 Å shift of TM7, thereby initiating signal transduction within the cell and activating heterotrimeric G proteins. It highlights the difference in engagement of the orthosteric site between C5a and the antagonist PMX53, with the former binding deeper within the pocket. Notably, the region around M265^{6,58} appears to be critical for the binding of β-arrestin to C5aR1. Moreover, previous literature has reported that β-arrestin predominantly binds to C5aR1 through its C-terminal P-X-PP motif. Given that the current structural data does not provide a clear view of the C-terminal P-X-PP structure, it is postulated that the M256A mutation may exert an influence on it. Moving forward, we will further investigate why the M265A mutation impedes downstream β-arrestin recruitment. These data suggest that design of a functionally selective compound could be achieved. This could be potentially advantageous to try and drive desensitization of the receptor or the opposite, to avoid arrestin driven internalization and signalling to favor cAMP production. Indeed, therapeutically, C5aR1 has been implicated in a number of immune-mediated diseases, including sepsis, acute lung injury, rheumatoid arthritis, and systemic lupus erythematosus. In these conditions, the activation of the C5aR1 can lead to excessive inflammation and tissue damage. C5aR1 is primarily expressed on the surface of immune cells, including neutrophils, monocytes, macrophages, and dendritic cells. The activation of the C5aR1 triggers a series of intracellular signaling events that lead to changes in the behavior and function of the immune cell. These changes include the release of inflammatory cytokines, the production of reactive oxygen species, and the enhancement of phagocytic activity. As a result, there has been significant interest

in developing therapeutics that target the C5aR1. One approach has been the development of small molecule antagonists that block the binding of C5a to the C5aR1. These antagonists have shown promise in preclinical models of inflammatory diseases, and several are currently in clinical development. Another approach has been the development of monoclonal antibodies that target the C5aR1. These antibodies can bind to the receptor and block its activation, as well as promote the internalization and degradation of the receptor. The structure reported here is complementary to previous documents,³⁹⁻⁴¹ and will directly aid the future development of both small molecules, peptides and biologics targeting this important receptor.

Materials and Methods

Molecular cloning

Based on previous studies, the wild-type C5a anaphylatoxin region (residues 678-751) of human complement C5 was synthesized into vector pFastBac utilizing codon optimization techniques. Similarly, the coding sequence of human wild-type complement receptor C5aR1 (residues 1-350) was cloned into pFastBac vector followed by 10×His tag and a LgBiT submit at C-terminus. Additionally, The Gβ1 was fused with a C-terminal HiBiT via a 12×GS linker. Furthermore, the Dominant-negative Gαi1 (DNGαi) and scFv16 were cloned into the pFastBac vector, while the Gβ1 was cloned into the pFastBac Dual vector. For the functional studies, human C5aR1 WT and mutants were synthesized by Twist Bioscience and cloned into their CMV vector.

Protein expression and purification

Using the Bac-to-Bac Expression System, recombinant viruses of C5a, C5aR1, DNGαi, Gβγ and scFv16 were produced and amplified in Sf9 cells. Sf9 cells at a density of 1-2×10⁶ cells/mL were infected with above five baculoviruses at a ratio of 1:1:1:1:1. Sf9 cells were cultured in suspension in a 27 °C constant temperature shaker. The cells were harvested after 48 hours of expressing the complex proteins by centrifugation at 3,000

rpm. Collected cells were stored at -80 °C for further purification. The cell pellets were resuspended in lysis buffer containing 25 mM HEPES (pH 7.5), 50 mM NaCl and EDTA-free protease inhibitor cocktail, and then disrupted using a tissue homogenizer. 25 mU/mL Apyrase (Sigma) was added and incubated for 1 hour at room temperature. After centrifugation at 40,000 rpm for 40 min, the supernatant was discarded. The resulting membrane pellets were resuspended in lysis buffer containing 25 mM HEPES (pH 7.5), 150 mM NaCl, 1%(w/v) lauryl maltose neopentyl glycol (LMNG) with 0.1%(w/v) cholesteryl hemisuccinate (CHS) and EDTA-free protease inhibitor cocktail. The mixture was then homogenized using the tissue homogenizer and incubated with gentle agitation for 3 hours at 4 °C to solubilize the membrane components. After centrifugation at 40,000 rpm for 40 min, supernatants were bound to Ni-NTA beads for 2 hours at 4 °C. The mixture was then transferred to a purification column and washed with buffer A [20 mM HEPES, 100 mM NaCl, 0.003%(w/v) LMNG/0.0003%(w/v) CHS, 20 mM imidazole, EDTA-free protease inhibitor cocktail] and buffer B [20 mM HEPES, 100 mM NaCl, 0.003% (w/v) LMNG/0.0003%(w/v) CHS, 50 mM imidazole, EDTA-free protease inhibitor cocktail] of 10 column volumes each, after which the supernatant was exhausted. Protein was then eluted with elution buffer [20 mM HEPES, 100 mM NaCl, 0.003%(w/v) LMNG/0.0003%(w/v) CHS, EDTA-free protease inhibitor cocktail] containing 300 mM imidazole. After concentration, the protein was further purified by Superose 6 Increase 10/300 GL column (GE Healthcare) in SEC buffer [20 mM HEPES, 100 mM NaCl, 0.003%(w/v) LMNG/0.0003%(w/v) CHS]. The peak fraction corresponding to the C5a-C5aR1-DNG α i protein was collected and concentrated to 5 mg/mL for electron microscopy experiments using a 100 kDa Centrifugal Filter Unit (Millipore).

Cryo-EM sample preparation and data acquisition

To prepare cryo-EM grid of the C5a-C5aR1-DNG α i complex, 3 μ L of samples at 5 mg/mL were added to 300 Mesh R1.2/1.3 Au Quantifoil grids (glow discharged at 15mA for 40 seconds with a Glow discharge cleaning system). Grid were blotted with qualitative filter paper in a Vitrobot Mark IV (Thermo Fisher Scientific) at 4 °C and 100% humidity for 3.5 second using a blot force of -2 prior to plunging into liquid

ethane. Cryo-EM grids were loaded on a Thermo Fisher Scientific 300 kV TEM Titan Krios equipped with Gatan K3 direct electron detector. Raw movies were collected in super-resolution mode at a magnification of 105,000, with a super-resolution pixel size of 0.415 Å. Each image was stored in 32-frame gain normalized stacks with a total dose of 46 e⁻/Å².

Cryo-EM data processing

For the C5a-C5aR1-DNGαi complex, a total of 2092 movies stacks were imported into cryoSPARC v3.3.2. After motion corrected, electron-dose weighted and CTF estimation, the initial particle was performed by cryoSPARC blob picker. 953,448 particles were selected after several rounds of 2D classification from 1,526,097 particles. The following ab initio reconstruction, heterogeneous refinement, and nonuniform refinement enable us to reconstruct the 3.52 Å structure with 217,636 particles, from which we generated the template to auto-pick particles. With processing 1,550,865 particles, the map quality was significantly improved with the application of heterogeneous refinement and nonuniform refinement, resulting in the final 3.41 Å map with 326,548 particles. To further improve the resolution, the final particle sets being used for nonuniform refinement from blob picker and template picker were combined after removing the duplicated particles, the following additional round heterogeneous refinement. The best class yielded a final dataset of 281,573 particles, which were re-extracted and applied for final nonuniform refinement and local refinement in cryoSPARC, a density map was obtained with overall resolution of 3.01 Å (determined by gold standard Fourier shell correlation (FSC) using the 0.143 criterion).

Model building and refinement for cryo-EM structures

The initial templates for resolving the structure of C5a-C5aR1-DNGαi were the crystal structure of C5aR1 (PDB ID C1Q) and the cryo-EM structure of the CCR1-Gαi complex (PDB ID 7VL8). The models were first docked into the cryo-EM density map of the C5aR1 complex using Chimera, and then iteratively manually adjusted and reconstructed in Coot and ISOLDE based on the cryo-EM electron density map. Realspace and reciprocal refinement, along with model statistical validation, were conducted using PHENIX. The statistics for 3D reconstruction and model refinement

are summarized in Table 1. Structural figures were exported using ChimeraX and PyMOL.

cAMP measurements

Human embryonic kidney 293 (HEK293) maintained in Dulbecco's Modified Eagle's Medium (DMEM)-high glucose (Sigma Aldrich). supplemented with penicillin (100 U/mL), streptomycin (100 µg/mL) and heat inactivated fetal bovine serum (FBS, 10%) (PAN-Biotech). The HEK293 cells were cultured using T75 flasks, with an area of growth of 75 cm² (CELLSTAR) (5% CO₂ atmosphere, 37 °C). Once the HEK293 cells had reached approximately 80% confluency, they were transiently transfected using reverse transfection with Lipofectamine 3000™ (ThermoFisher) per the manufactures guidance in white clear bottom 96-well plate (Greiner Bio-One) coated with poly-D-lysine (Sigma-Aldrich). The plate was then incubated (5% CO₂ atmosphere, 37 °C, 24 hours) prior to performing cell signalling assays. After 24 hours of incubation, the transfected HEK293 cells were then subject to starvation in DMEM containing no supplementation of antibiotics or FBS for 2 hours. The 96-well plate was then incubated (5% CO₂ atmosphere, 37 °C, 2 hours). Cells were then equilibrated in cAMP Buffer (1× HBSS, 24 mM HEPES, 0.1% (w/v) BSA, 3.96 mM NaHCO₃, 1 mM MgSO₄, 1.3 mM CaCl₂·2H₂O), supplemented with Firefly D-Luciferin free acid (0.45 mg/mL) (NanoLight Technology). The 96-well plate was then incubated (28 °C, 1 hour). Luminescence was then measured using the CLARIOstar® Plus Plate Reader (BMG LabTech, Germany). Prior to injecting C5a (R&D Systems), approximately 5-10 basal readings were performed until stabilization was reached. Luminescence was measured for a total of 45 cycles (1 minute per cycle, 1 second integration time, without filter, a fixed gain of 3,000 and auto-focus).

Arrestin recruitment assays

β-arrestin 2 recruitment to the plasma membrane was measured using a bystander NanoBiT-β-arrestin assay using SmBiT-β-arrestin and LgBiT-CAAX constructs. Human embryonic kidney 293 (HEK293) adherent cells were passaged and transfected as above with a plasmid mixture consisting of 2.5 ng SmBiT-β-arrestin 2, 12.5 ng of LgBiT-CAAX and 100 ng of C5aR1 construct in Opti-MEM (Thermo Fisher

Scientific). The transfection mix (50 μL /well) was added to a white bottom 96-well plate (Costar) coated with poly-D-lysine (Sigma-Aldrich) followed by HEK293 cell suspension (100 μL /well). The plate was then incubated (5% CO_2 atmosphere, 37 $^\circ\text{C}$, 24 hours) prior to performing cell signalling assays. After 24 hours of incubation, the transfected HEK293 cells were removed from the wells and equilibrated with standard buffer (1 \times HBSS, 24 mM HEPES, 0.1% (w/v) BSA, 3.96 mM NaHCO_3 , 1 mM MgSO_4 , 1.3 mM $\text{CaCl}_2 \cdot 2\text{H}_2\text{O}$, 90 μL) for 1 hour at 37 $^\circ\text{C}$. After incubation, NanoFuel[®] GLOW Assay for Oplophorus Luciferases (25 μL) was then added to all wells. Bioluminescence was then measured using the CLARIOstar[®] Plus Plate Reader (BMG LabTech, Germany). Prior to injecting the treatment ligands, approximately 3-5 basal readings were performed until stabilization was reached. Bioluminescence was measured for a total of 30 cycles (1 minute per cycle, 1 second integration time, without filter, a fixed gain of 3,000 and auto-focus).

Acknowledgements and Funding

We would like to thank the Cryo-EM center of Southern University of Science and Technology for our Cryo-EM work and their help of Cryo-EM data collection. J.Z. was supported by the National Natural Science Foundation of China (grant no. 32271260; grant no. 81974514), and the Jiangxi Province Natural Science Foundation (grant no. 20224ACB206046). Y.L. is an investigator of SUSTech Institute for Biological Electron Microscopy. Y.L. was supported by the National Natural Science Foundation of China (grant no.32322004; grant no. 32171205; grant no. U22A20338), and the Shenzhen Natural Science Foundation (grant no.20220815130429001. J.L. was supported by the Open Project of Key Laboratory of Prevention and treatment of cardiovascular and cerebrovascular diseases, Ministry of Education (No. XN201904), Gannan Medical University (QD201910), Jiangxi key research and development program (20203BBG73063) and Jiangxi "Double Thousand Plan". P.J.M was supported by the Foreign Talent project of Jiangxi Province and BBSRC BB/R006946/1 and BB/V00719X/1. F.Y. was supported by Shenzhen Science and Technology Program (JCYJ20210324115611032 and KQTD20200909113758004). H.J. was supported by the National Natural Science Foundation of China (32360223) and Jiangxi Provincial Natural Science Foundation (20224BAB216004 and 20232BAB205025). This work was also supported by Ganzhou COVID-19 Emergency Research Project (2020.17), Major science and technology programs of Ganzhou City (2020.67) and Ganzhou Zhanggong District COVID-19 prevention and control key research projects (2020.67).

Author Contributions

Tingting Yang: Investigation, Formal analysis, Writing – original draft. Jian Li: Investigation, Project administration. Xinyu Cheng: Methodology, Investigation. Qiuyuan Lu: Investigation, Formal analysis. Zara Farooq: Data curation, Investigation. Ying Fu: Investigation. Sijia Lv: Investigation. Weiwei Nan: Investigation. Boming Yu: Investigation. Jingjing Duang: Writing – review & editing. Yuting Zhang: Investigation. Yang Fu: Data curation, Writing – review & editing. Haihai Jiang: Formal analysis, Writing – review & editing, Supervision. Peter J McCormick: Supervision. Yanyan Li: Supervision. Jin Zhang: Supervision, Project administration, Writing – review & editing, Conceptualization.

Declaration of Interest

The authors declare no conflict of interest.

Data availability

Data deposition: Cryo-EM electron density map of the human C5a-C5aR1-Gi complex has been deposited in the Electron Microscopy Data Bank, <https://www.ebi.ac.uk/pdbe/emdb/35587>), and the fitted coordinate has been deposited in the Protein Data Bank, www.pdb.org (PDB ID 8IN5). The data that support the findings of this study are available from the corresponding author upon reasonable request.

References

- Ajona, D., Ortiz-Espinosa, S., & Pio, R. (2019). Complement anaphylatoxins C3a and C5a: Emerging roles in cancer progression and treatment. *Semin Cell Dev Biol*, 85, 153-163. <https://doi.org/10.1016/j.semcdb.2017.11.023>
- An, G., Ren, G., An, F., & Zhang, C. (2014). Role of C5a-C5aR axis in the development of atherosclerosis. *Sci China Life Sci*, 57(8), 790-794. <https://doi.org/10.1007/s11427-014-4711-5>
- Anliker-Ort, M., Dingemans, J., van den Anker, J., & Kaufmann, P. (2020). Treatment of Rare Inflammatory Kidney Diseases: Drugs Targeting the Terminal Complement Pathway. *Front Immunol*, 11, 599417. <https://doi.org/10.3389/fimmu.2020.599417>
- Arbore, G., West, E. E., Spolski, R., Robertson, A. A. B., Klos, A., Rheinheimer, C., Dutow, P., Woodruff, T. M., Yu, Z. X., O'Neill, L. A., Coll, R. C., Sher, A., Leonard, W. J., Kohl, J., Monk, P., Cooper, M. A., Arno, M., Afzali, B., Lachmann, H. J., Cope, A. P., Mayer-Barber, K. D., & Kemper, C. (2016). T helper 1 immunity requires complement-driven NLRP3 inflammasome activity in CD4(+) T cells. *Science*, 352(6292), aad1210. <https://doi.org/10.1126/science.aad1210>
- Ardissino, G., Capone, V., Tedeschi, S., Porcaro, L., & Cugno, M. (2022). Complement System as a New Target for Hematopoietic Stem Cell Transplantation-Related Thrombotic Microangiopathy. *Pharmaceuticals (Basel)*, 15(7). <https://doi.org/10.3390/ph15070845>
- Bruchfeld, A., Magin, H., Nachman, P., Parikh, S., Lafayette, R., Potarca, A., Miao, S., & Bekker, P. (2022). C5a receptor inhibitor avacopan in immunoglobulin A nephropathy-an open-label pilot study. *Clin Kidney J*, 15(5), 922-928. <https://doi.org/10.1093/ckj/sfab294>
- Buhl, A. M., Avdi, N., Worthen, G. S., & Johnson, G. L. (1994). Mapping of the C5a receptor signal transduction network in human neutrophils. *Proc Natl Acad Sci U S A*, 91(19), 9190-9194. <https://doi.org/10.1073/pnas.91.19.9190>
- Darling, V. R., Hauke, R. J., Tarantolo, S., & Agrawal, D. K. (2015). Immunological effects and therapeutic role of C5a in cancer. *Expert Rev Clin Immunol*, 11(2), 255-263. <https://doi.org/10.1586/1744666X.2015.983081>
- Duan, J., Shen, D. D., Zhou, X. E., Bi, P., Liu, Q. F., Tan, Y. X., Zhuang, Y. W., Zhang, H. B., Xu, P. Y., Huang, S. J., Ma, S. S., He, X. H., Melcher, K., Zhang, Y., Xu, H. E., & Jiang, Y. (2020). Cryo-EM structure of an activated VIP1 receptor-G protein complex revealed by a NanoBiT tethering strategy. *Nat Commun*, 11(1), 4121. <https://doi.org/10.1038/s41467-020-17933-8>
- Fattahi, F., Zetoune, F. S., & Ward, P. A. (2020). Complement as a Major Inducer of Harmful Events in Infectious Sepsis. *Shock*, 54(5), 595-605. <https://doi.org/10.1097/SHK.0000000000001531>
- Feng, Y., Zhao, C., Deng, Y., Wang, H., Ma, L., Liu, S., Tian, X., Wang, B., Bin, Y., Chen, P., Yan, W., Fu, P., & Shao, Z. (2023). Mechanism of activation and biased signaling in complement receptor C5aR1. *Cell Res*, 33(4), 312-324. <https://doi.org/10.1038/s41422-023-00779-2>
- Gabilan, C., Pfirmann, P., Ribes, D., Rigother, C., Chauveau, D., Casemayou, A., Huart, A., Schanstra, J., Colombat, M., Faguer, S., & Belliere, J. (2022). Avacopan as First-Line Treatment in Antineutrophil Cytoplasmic Antibody-Associated Vasculitis: A Steroid-Sparing Option. *Kidney Int Rep*, 7(5), 1115-1118. <https://doi.org/10.1016/j.ekir.2022.01.1065>
- Harigai, M., & Takada, H. (2022). Avacopan, a selective C5a receptor antagonist, for anti-neutrophil cytoplasmic antibody-associated vasculitis. *Mod Rheumatol*, 32(3), 475-483. <https://doi.org/10.1093/mr/roab104>
- Hauser, A. S., Attwood, M. M., Rask-Andersen, M., Schioth, H. B., & Gloriam, D. E. (2017). Trends

- in GPCR drug discovery: new agents, targets and indications. *Nat Rev Drug Discov*, 16(12), 829-842. <https://doi.org/10.1038/nrd.2017.178>
- Hauser, A. S., Chavali, S., Masuho, I., Jahn, L. J., Martemyanov, K. A., Gloriam, D. E., & Babu, M. M. (2018). Pharmacogenomics of GPCR Drug Targets. *Cell*, 172(1-2), 41-54.e19. <https://doi.org/10.1016/j.cell.2017.11.033>
- Helske, S., Oksjoki, R., Lindstedt, K. A., Lommi, J., Turto, H., Werkkala, K., Kupari, M., & Kovanen, P. T. (2008). Complement system is activated in stenotic aortic valves. *Atherosclerosis*, 196(1), 190-200. <https://doi.org/10.1016/j.atherosclerosis.2007.03.040>
- Horiuchi, T., & Tsukamoto, H. (2016). Complement-targeted therapy: development of C5- and C5a-targeted inhibition. *Inflamm Regen*, 36, 11. <https://doi.org/10.1186/s41232-016-0013-6>
- Huang, H., & Tao, Y. X. (2014). Functions of the DRY motif and intracellular loop 2 of human melanocortin 3 receptor. *J Mol Endocrinol*, 53(3), 319-330. <https://doi.org/10.1530/jme-14-0184>
- Jayne, D. R. W., Merkel, P. A., Schall, T. J., & Bekker, P. (2021). Avacopan for the Treatment of ANCA-Associated Vasculitis. *N Engl J Med*, 384(7), 599-609. <https://doi.org/10.1056/NEJMoa2023386>
- Klos, A., Tenner, A. J., Johswich, K. O., Ager, R. R., Reis, E. S., & Kohl, J. (2009). The role of the anaphylatoxins in health and disease. *Mol Immunol*, 46(14), 2753-2766. <https://doi.org/10.1016/j.molimm.2009.04.027>
- Köhl, J. (2006). Drug evaluation: the C5a receptor antagonist PMX-53. *Curr Opin Mol Ther*, 8(6), 529-538.
- Lee, A. (2022). Avacopan: First Approval. *Drugs*, 82(1), 79-85. <https://doi.org/10.1007/s40265-021-01643-6>
- Li, J., & Liu, B. (2021). The roles and potential therapeutic implications of C5a in the pathogenesis of COVID-19-associated coagulopathy. *Cytokine Growth Factor Rev*, 58, 75-81. <https://doi.org/10.1016/j.cytogfr.2020.12.001>
- Liu, H., Kim, H. R., Deepak, R., Wang, L., Chung, K. Y., Fan, H., Wei, Z., & Zhang, C. (2018). Orthosteric and allosteric action of the C5a receptor antagonists. *Nat Struct Mol Biol*, 25(6), 472-481. <https://doi.org/10.1038/s41594-018-0067-z>
- Liu, H., Sun, D., Myasnikov, A., Damian, M., Baneres, J. L., Sun, J., & Zhang, C. (2021). Structural basis of human ghrelin receptor signaling by ghrelin and the synthetic agonist ibutamoren. *Nat Commun*, 12(1), 6410. <https://doi.org/10.1038/s41467-021-26735-5>
- Maharana, J., & Shukla, A. K. (2021). Feeling at home: Structure of the NTSR1-G(i) complex in a lipid environment. *Nat Struct Mol Biol*, 28(4), 331-333. <https://doi.org/10.1038/s41594-021-00581-x>
- Marceau, F., & Petitcherc, E. (2022). C5a receptor antagonism coming of age for vascular pathology. *Int Immunopharmacol*, 110, 109042. <https://doi.org/10.1016/j.intimp.2022.109042>
- Matsumoto, I., Muraki, Y., Yasukochi, T., Hua, Z., Kori, Y., Hayashi, T., Goto, D., Ito, S., Tsutsumi, A., Ikeda, K., Sumichika, H., & Sumida, T. (2005). The exploration of joint-specific immunoreactions on immunoglobulins G of anti-glucose-6-phosphate isomerase antibody-positive patients with rheumatoid arthritis. *Int J Mol Med*, 16(5), 793-800.
- Mehta, G., Scheinman, R. I., Holers, V. M., & Banda, N. K. (2015). A New Approach for the Treatment of Arthritis in Mice with a Novel Conjugate of an Anti-C5aR1 Antibody and C5 Small Interfering RNA. *J Immunol*, 194(11), 5446-5454. <https://doi.org/10.4049/jimmunol.1403012>
- Merle, N. S., Noe, R., Halbwachs-Mecarelli, L., Fremeaux-Bacchi, V., & Roumenina, L. T. (2015).

- Complement System Part II: Role in Immunity. *Front Immunol*, 6, 257. <https://doi.org/10.3389/fimmu.2015.00257>
- Paczkowski, N. J., Finch, A. M., Whitmore, J. B., Short, A. J., Wong, A. K., Monk, P. N., Cain, S. A., Fairlie, D. P., & Taylor, S. M. (1999). Pharmacological characterization of antagonists of the C5a receptor. *Br J Pharmacol*, 128(7), 1461–1466.
- Pandey, S., Li, X. X., Srivastava, A., Baidya, M., Kumari, P., Dwivedi, H., Chaturvedi, M., Ghosh, E., Woodruff, T. M., & Shukla, A. K. (2019). Partial ligand-receptor engagement yields functional bias at the human complement receptor, C5aR1. *J Biol Chem*, 294(24), 9416-9429. <https://doi.org/10.1074/jbc.RA119.007485>
- Perianayagam, M. C., Balakrishnan, V. S., King, A. J., Pereira, B. J., & Jaber, B. L. (2002). C5a delays apoptosis of human neutrophils by a phosphatidylinositol 3-kinase-signaling pathway. *Kidney Int*, 61(2), 456-463. <https://doi.org/10.1046/j.1523-1755.2002.00139.x>
- Quadros, A. U., & Cunha, T. M. (2016). C5a and pain development: An old molecule, a new target. *Pharmacol Res*, 112, 58-67. <https://doi.org/10.1016/j.phrs.2016.02.004>
- Ricklin, D., & Lambris, J. D. (2007). Complement-targeted therapeutics. *Nat Biotechnol*, 25(11), 1265-1275. <https://doi.org/10.1038/nbt1342>
- Robertson, N., Rappas, M., Doré, A. S., Brown, J., Bottegoni, G., Koglin, M., Cansfield, J., Jazayeri, A., Cooke, R. M., & Marshall, F. H. (2018). Structure of the complement C5a receptor bound to the extra-helical antagonist NDT9513727. *Nature*, 553(7686), 111-114. <https://doi.org/10.1038/nature25025>
- Sadik, C. D., Miyabe, Y., Sezin, T., & Luster, A. D. (2018). The critical role of C5a as an initiator of neutrophil-mediated autoimmune inflammation of the joint and skin. *Semin Immunol*, 37, 21-29. <https://doi.org/10.1016/j.smim.2018.03.002>
- Schanzenbacher, J., Kohl, J., & Karsten, C. M. (2022). Anaphylatoxins spark the flame in early autoimmunity. *Front Immunol*, 13, 958392. <https://doi.org/10.3389/fimmu.2022.958392>
- Schatz-Jakobsen, J. A., Yatime, L., Larsen, C., Petersen, S. V., Klos, A., & Andersen, G. R. (2014). Structural and functional characterization of human and murine C5a anaphylatoxins. *Acta Crystallogr D Biol Crystallogr*, 70(Pt 6), 1704–1717.
- Shao, Z., Shen, Q., Yao, B., Mao, C., Chen, L. N., Zhang, H., Shen, D. D., Zhang, C., Li, W., Du, X., Li, F., Ma, H., Chen, Z. H., Xu, H. E., Ying, S., Zhang, Y., & Shen, H. (2022). Identification and mechanism of G protein-biased ligands for chemokine receptor CCR1. *Nat Chem Biol*, 18(3), 264-271. <https://doi.org/10.1038/s41589-021-00918-z>
- Shi, Y., Chen, X., Liu, J., Fan, X., Jin, Y., Gu, J., Liang, J., Liang, X., & Wang, C. (2021). Isoquercetin Improves Inflammatory Response in Rats Following Ischemic Stroke. *Front Neurosci*, 15, 555543. <https://doi.org/10.3389/fnins.2021.555543>
- Solino, M., Larrayoz, I. M., Lopez, E. M., Rey-Funes, M., Bareiro, M., Loidl, C. F., Girardi, E., Martinez, A., & Lopez-Costa, J. J. (2022). Adenosine A2A Receptor: A New Neuroprotective Target in Light-Induced Retinal Degeneration. *Front Pharmacol*, 13, 840134. <https://doi.org/10.3389/fphar.2022.840134>
- Sommerfeld, O., Medyukhina, A., Neugebauer, S., Ghait, M., Ulferts, S., Lupp, A., Konig, R., Wetzker, R., Schulz, S., Figge, M. T., Bauer, M., & Press, A. T. (2021). Targeting Complement C5a Receptor 1 for the Treatment of Immunosuppression in Sepsis. *Mol Ther*, 29(1), 338-346. <https://doi.org/10.1016/j.ymthe.2020.09.008>
- Sun, C., Wang, B., & Hao, S. (2022). Adenosine-A2A Receptor Pathway in Cancer Immunotherapy.

Front Immunol, 13, 837230. <https://doi.org/10.3389/fimmu.2022.837230>

Talaat, I. M., Elemam, N. M., & Saber-Ayad, M. (2022). Complement System: An Immunotherapy Target in Colorectal Cancer. *Front Immunol*, 13, 810993. <https://doi.org/10.3389/fimmu.2022.810993>

Tampe, D., Hakroush, S., & Tampe, B. (2022). Molecular signatures of intrarenal complement receptors C3AR1 and C5AR1 correlate with renal outcome in human lupus nephritis. *Lupus Sci Med*, 9(1). <https://doi.org/10.1136/lupus-2022-000831>

Vigano, S., Alatzoglou, D., Irving, M., Menetrier-Caux, C., Caux, C., Romero, P., & Coukos, G. (2019). Targeting Adenosine in Cancer Immunotherapy to Enhance T-Cell Function. *Front Immunol*, 10, 925. <https://doi.org/10.3389/fimmu.2019.00925>

Wang, Y., Liu, W., Xu, Y., He, X., Yuan, Q., Luo, P., Fan, W., Zhu, J., Zhang, X., Cheng, X., Jiang, Y., Xu, H. E., & Zhuang, Y. (2023). Revealing the signaling of complement receptors C3aR and C5aR1 by anaphylatoxins. *Nat Chem Biol*, 19(11), 1351-1360. <https://doi.org/10.1038/s41589-023-01339-w>

West, E. E., Kolev, M., & Kemper, C. (2018). Complement and the Regulation of T Cell Responses. *Annu Rev Immunol*, 36, 309-338. <https://doi.org/10.1146/annurev-immunol-042617-053245>

Woodruff, T. M., Nandakumar, K. S., & Tedesco, F. (2011). Inhibiting the C5-C5a receptor axis. *Mol Immunol*, 48(14), 1631-1642. <https://doi.org/10.1016/j.molimm.2011.04.014>

Yadav, M. K., Maharana, J., Yadav, R., Saha, S., Sarma, P., Soni, C., Singh, V., Saha, S., Ganguly, M., Li, X. X., Mohapatra, S., Mishra, S., Khant, H. A., Chami, M., Woodruff, T. M., Banerjee, R., Shukla, A. K., & Gati, C. (2023). Molecular basis of anaphylatoxin binding, activation, and signaling bias at complement receptors. *Cell*, 186(22), 4956-4973.e4921. <https://doi.org/10.1016/j.cell.2023.09.020>

Yang, L. K., & Tao, Y. X. (2020). Alanine Scanning Mutagenesis of the DRYxxI Motif and Intracellular Loop 2 of Human Melanocortin-4 Receptor. *Int J Mol Sci*, 21(20). <https://doi.org/10.3390/ijms21207611>

Zhang, X., Hu, J., Becker, K. V., Engle, J. W., Ni, D., Cai, W., Wu, D., & Qu, S. (2021). Antioxidant and C5a-blocking strategy for hepatic ischemia-reperfusion injury repair. *J Nanobiotechnology*, 19(1), 107. <https://doi.org/10.1186/s12951-021-00858-9>

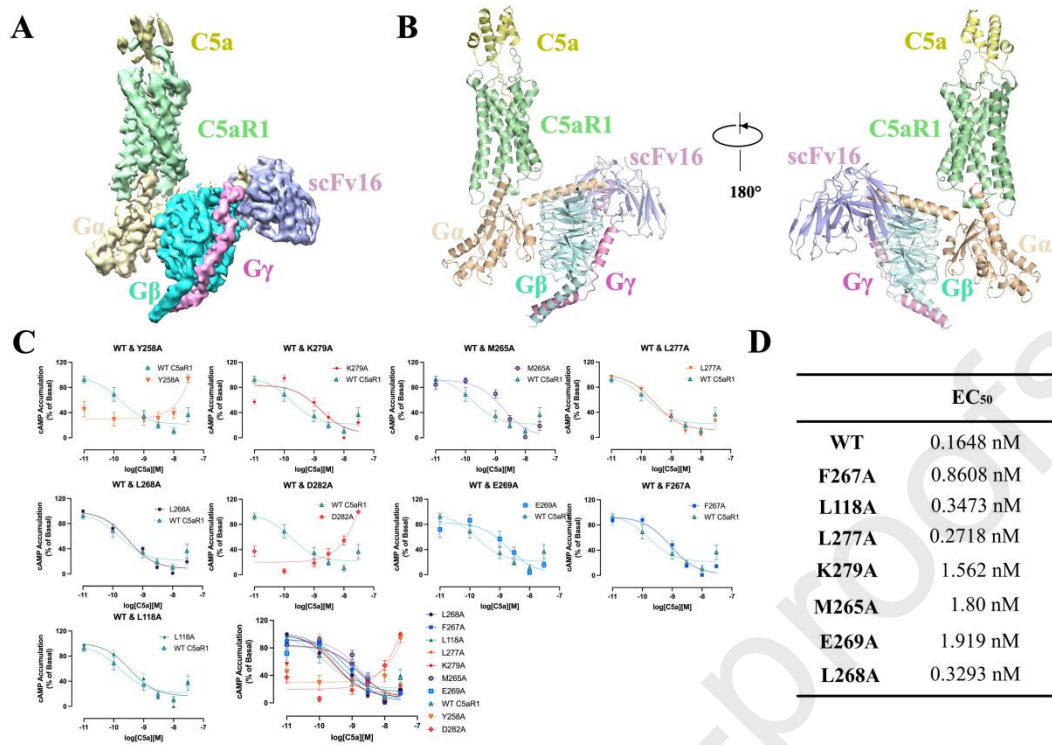


Figure 1 Overall structure of C5a-C5aR1-Gi complex. (A) Cryo-EM density map of human C5a-C5aR1-Gi. (B) Two ribbon diagrams of the human C5a-C5aR1-Gi complex model are presented in side views, with C5a, C5aR1, G α i, G β , and G γ colored in yellow, green, wheat, cyan, and magenta, respectively. Each subunit is labeled with its name. (C) The inhibition of forskolin induced cAMP production was measured in HEK 293 cells by using a real-time cAMP pGlo biosensor to activate nine C5aR1 mutants, including L118A, Y258A, M265A, F267A, L268A, E269A, L277A, K279A and D282A. (D) The EC₅₀ values for the wild-type C5aR1 and nine mutations were determined in the aforementioned experiments.

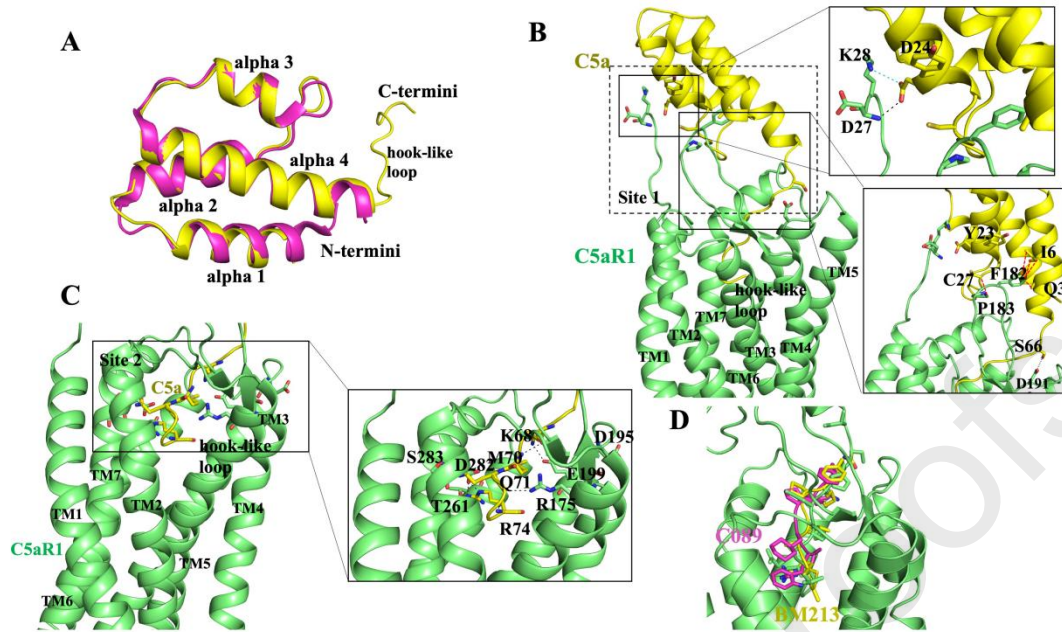


Figure 2 C5a binding site. (A) Comparison between the structure of C5a (yellow) in our cryo-EM structure and the previous reported crystal structure of C5a (magenta; PDB ID 4P3A) is shown. (B and C) Two sites are presented. Site 1: a polar recognition region on the extracellular side (B), where the structure of C5a (yellow) interacts extensively with the N-terminus and extracellular loop 2 (ECL2) of C5aR1 (green). Salt bridge is shown as cyan dashed line. Hydrogen bond is shown in black dashed lines. Hydrophobic interactions are shown in red dashed lines. Site 2: an amphipathic pocket within the transmembrane domain composed of TM2, TM3 and TM5-7 in C5aR1 (green) (C). (D) Small molecules BM213 peptide (yellow) and C089 peptide (pink) bind in the same pocket as C5a (green) (PDB IDs 7Y66 and 7Y67).

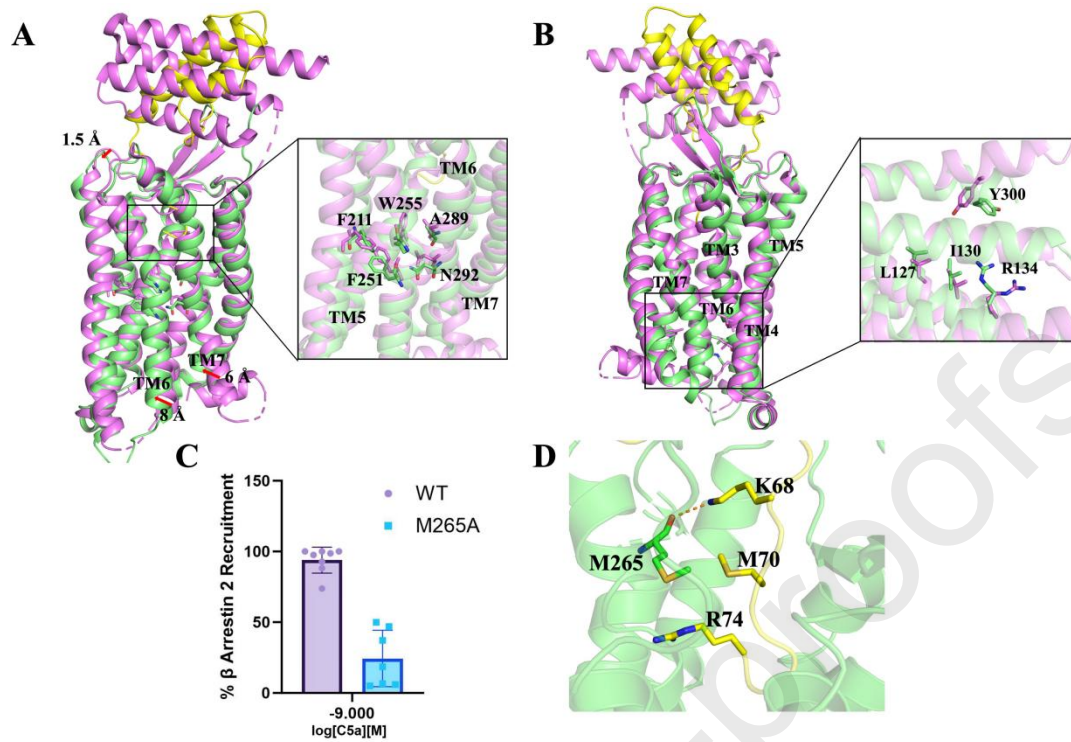


Figure 3 Receptor activation mechanism of C5aR1. (A) TM6-7 in our C5aR1 structure (green) was compared with that in previously solved crystal structure of C5aR1 (left; violet; PDB ID 6C1Q), revealing a shift in F211^{5.51}, F251^{6.44}, A289^{7.42}, N292^{7.45}, and W255^{6.48} (right). (B) Comparison of TM3-7 between the two structures (left). Y300^{7.53} undergoes a significant displacement towards the intracellular core, resulting in an inward movement of TM7 (right). (C) The mutation of M265^{6.58} completely abrogated the recruitment of β -arrestin 2. (D) The interaction between M265 in C5aR1 and the residues K68, M70 and R74 in C5a. Hydrogen bonding interaction is shown in dashed line.

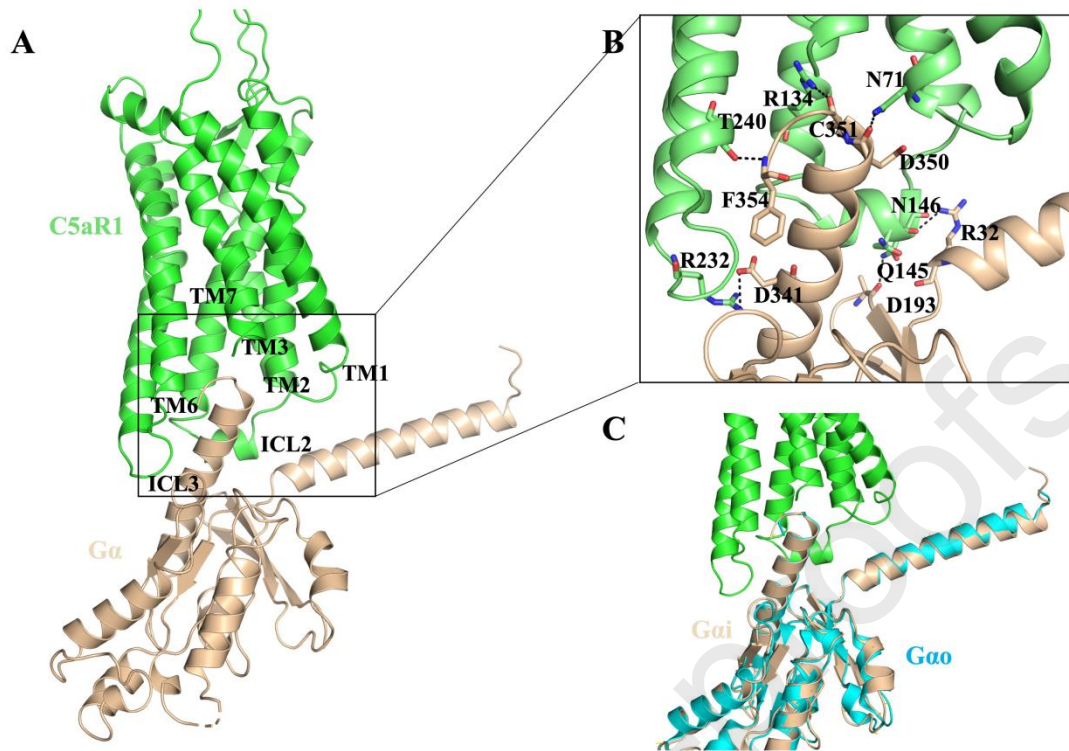


Figure 4 C5aR1-Gi complex interface. (A) Side view of the interface between C5aR1 (green) and Gi (wheat), which is formed by the cytoplasmic ends of TM3, TM6, TM7, ICL2, and ICL3. The close proximity of these structural elements creates a complex network of interactions that are essential for the proper functioning of the complex. (B) Interactions between C5aR1 (green) and Gi (wheat). Specifically, several residues contribute to the stabilization of the complex structure and maintenance of its orientation through the formation of hydrogen bonds and hydrophobic forces. These interactions are crucial for downstream signaling pathways to be activated. (C) Comparison of the interaction interface with C5aR1-Gao (PDB ID 8IA2).

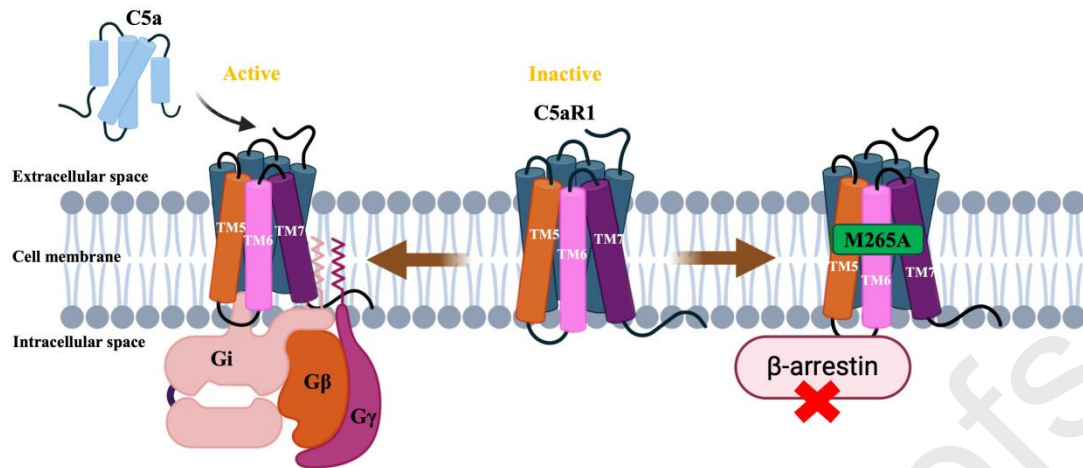


Figure 5 Schematic model of C5aR1 activation by C5a and M265. The activation mechanism of ligand C5a binding to C5aR1 involves displacement of TM6 outward by about 8.0 Å and inward shifting of TM7 by about 6.0 Å when C5a combines with C5aR1. These structural changes are typical for GPCRs and enable downstream signaling pathways to activate. Despite of no significant change in G-protein driven signaling, mutation of M265^{6,58} completely abrogated β-arrestin 2 recruitment.

Supplementary Figures

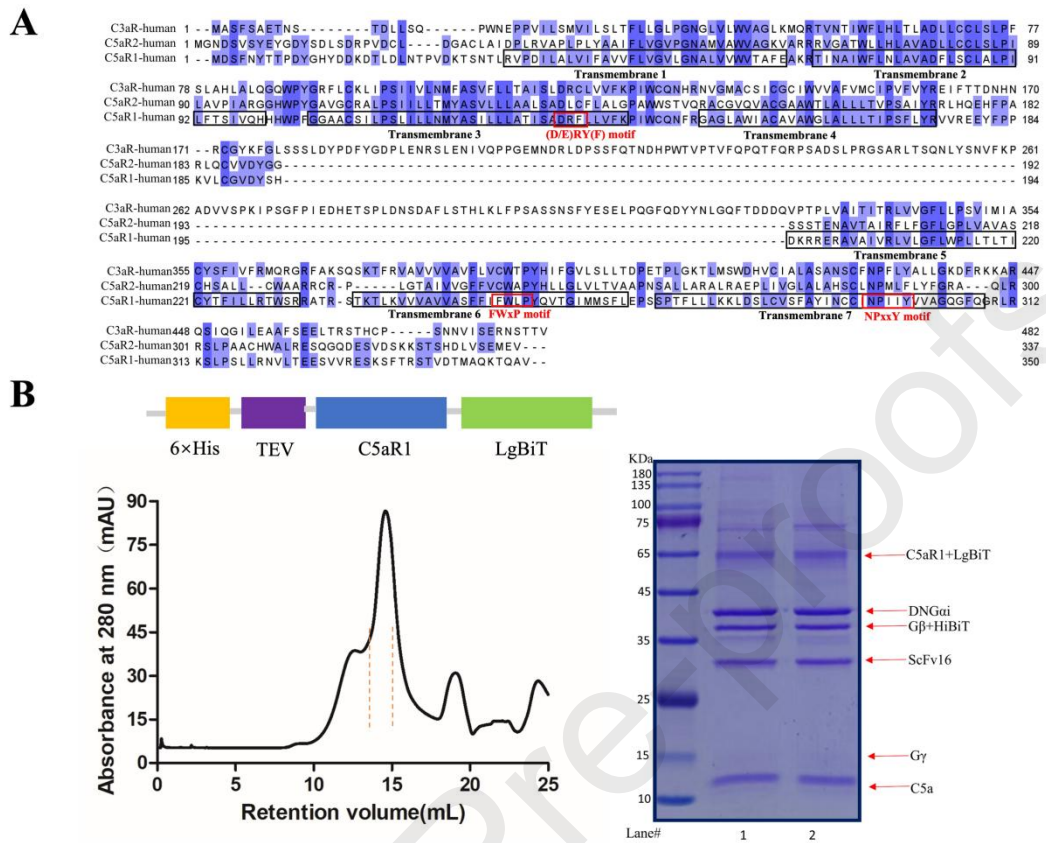


Figure S1 The biochemical characterization of C5a-C5aR1-C5aR1-Gi complex construct. (A) Sequence of the full-length human C5aR1 aligned with other complement subfamily members are shown. Key residues were indicated and transmembrane helices were labeled. Clustal Omega was used for sequence alignments. (B) Size exclusion chromatography of the C5a-C5aR1-Gi complex. Retention volume and the peak corresponding to C5a-C5aR1-Gi complex are indicated (left). Protein samples from the indicated C5a-C5aR1-Gi complex protein fraction were subjected to SDS-PAGE and Coomassie-blue staining, with lane 1 and 2 containing protein collected from the target peak.

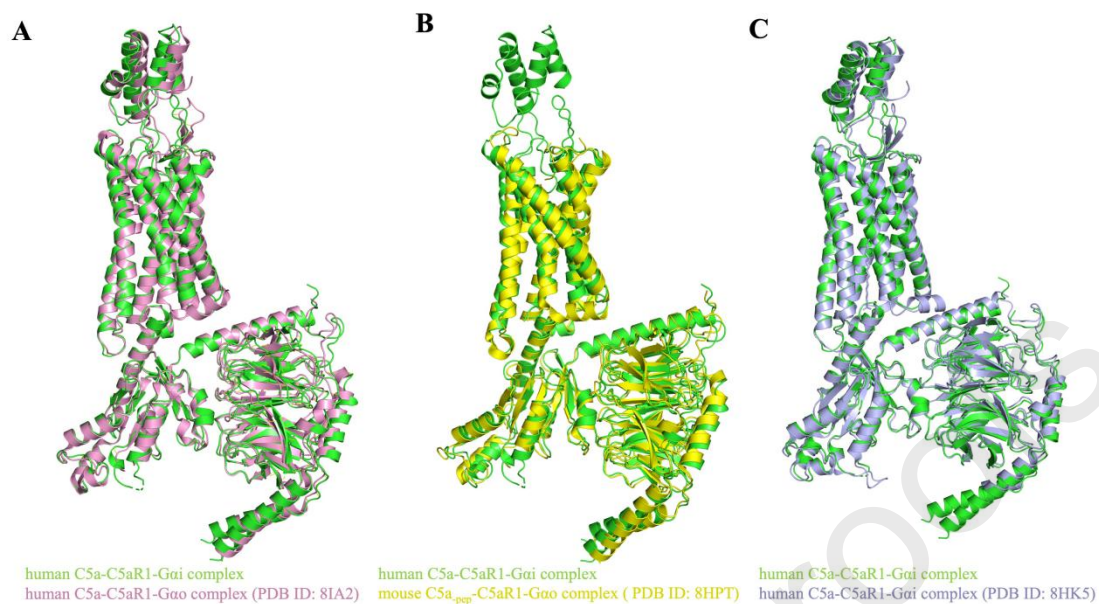


Figure S2 Structural comparison of C5aR1-C5a-G complexes. (A) Comparison of our human C5a-C5aR1-G α i structure (green) with the structure of human C5a-C5aR1-G α o complex (pink, PDB ID 8IA2). (B) Comparison of our structure with the structure of mouse C5a-pep-C5aR1-G α o complex (yellow, PDB ID 8HPT). (C) Comparison of our structure with the structure of human C5a-C5aR1-G α i complex (light-blue, PDB ID 8HK5).

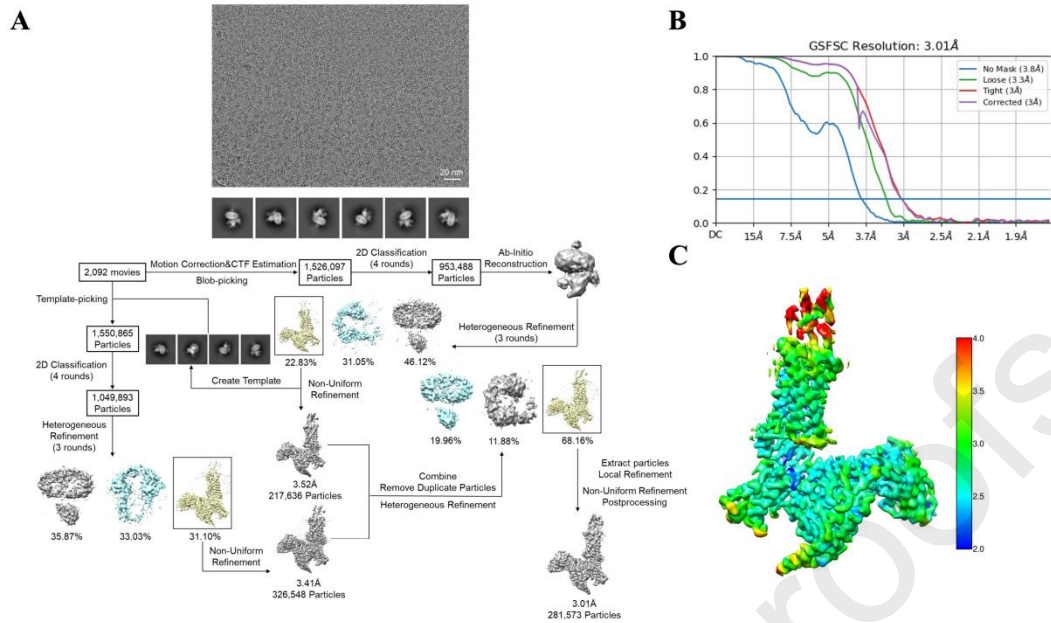


Figure S3 Flow chart for cryo-EM data processing and structure determination. (A) Representative image of the purified C5a-C5aR1-Gi complex protein, including 2D class averages of complex particles (top), side views of the 3D reconstructions from cryoSPARC 3D classification and final 3D reconstructions from 3D auto-refinement (bottom). (B) The Fourier shell correlation (FSC) curve of the complex protein 3D reconstruction, showing an overall resolution at 3.0 Å. (C) Local resolution estimation of C5a-C5aR1-Gi complex.

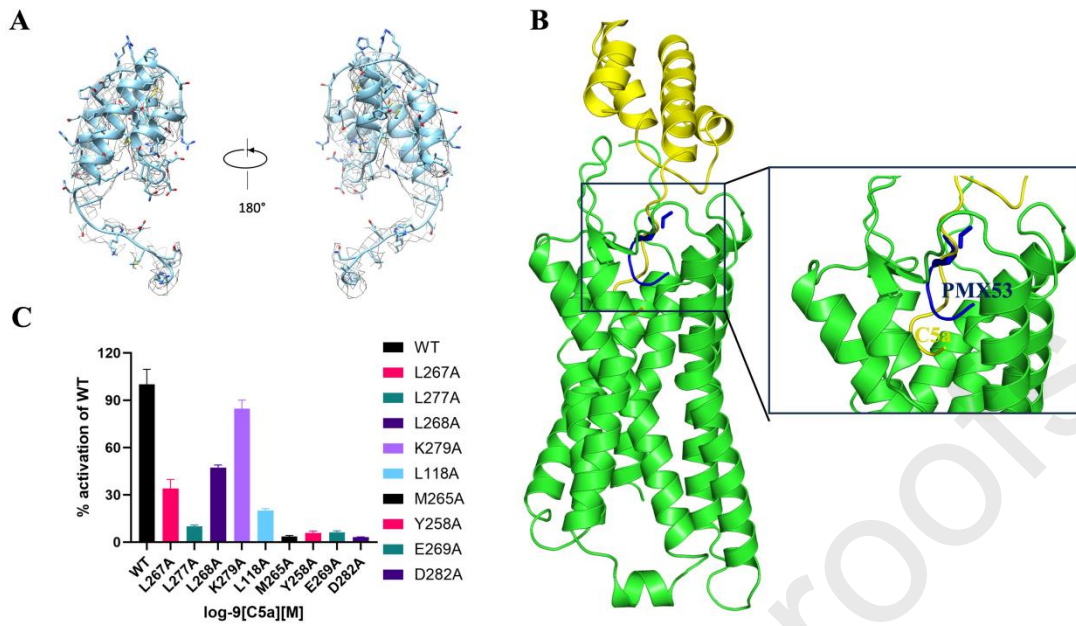


Figure S4 The density map of C5a and the distinctions between the binding pocket of C5a and PMX53 in C5aR1. (A) Two perspectives of the density map of C5a. (B) A comparison of the small-molecule antagonist PMX53 (PDB ID 6C1R) and C5a in the binding pocket of C5aR1. PMX53 is colored in blue, while C5a in yellow and C5aR1 in green. (C) β -arrestin2 recruitment results of the wild-type C5aR1 and its nine mutated variants.

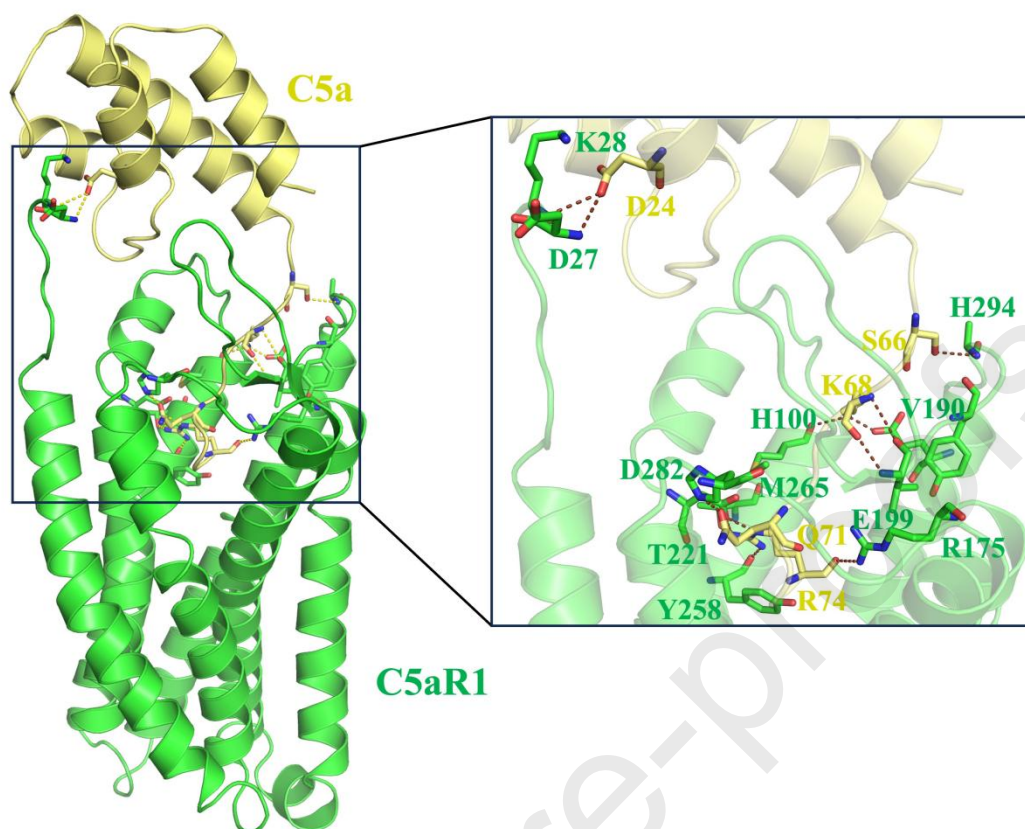


Figure S5 Key residues involved in the interaction between C5a and C5aR1. C5a and C5aR1 are colored in yellow and green, respectively. Key residues include K68, M70, Q71, G73, R74 of C5a, and E269, F267, M265, D282, Y258 of C5aR1. Salt bridges or hydrogen bonds are indicated as black dashed lines.

Table 1. Cryo-EM data collection, refinement and validation statistics

	C5a-C5aR1-DNGi (EMD35587) (PDB 8IN5)
Data collection and processing	
Magnification	105,000
Voltage (kV)	300
Electron exposure ($e^-/\text{\AA}^2$)	46
Defocus range (μm)	-1.8 - -2.2
Pixel size (\AA)	0.83
Symmetry imposed	<i>C1</i>
Initial particle images (no.)	1,550,865
Final particle images (no.)	281,573
Map resolution (\AA)	3.01

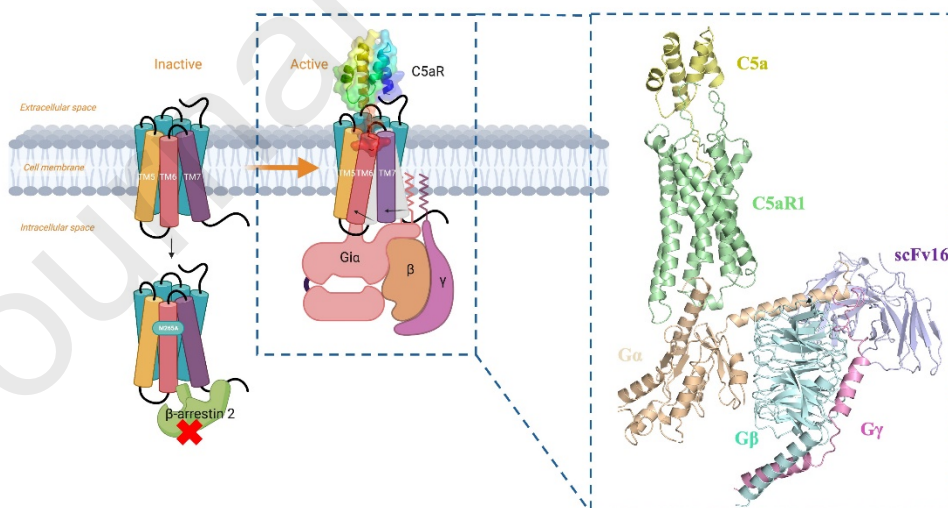
Refinement	
Initial model used (PDB code)	7VL8
Model resolution (Å)	3.0
Model composition	
Non-hydrogen atoms	7440
Protein residues	952
Ligands	0
R.m.s. deviations	
Bond lengths (Å)	0.0143
Bond angles (°)	1.37
Validation	
MolProbity score	1.69
Ramachandran plot	
Favored (%)	96.22
Allowed (%)	3.78
Disallowed (%)	0.00

Research Highlights

- The structure of human C5a-C5aR1-Gi was determined at a high resolution of 3 Å.
- Structure analysis revealed the mechanism of C5aR1 activation.
- M265 on transmembrane helix 6 of C5aR plays a crucial role in recruiting β -arrestin.

Schematic model of C5aR1 activation by C5a

Structure of human C5a-C5aR1 complex



Declaration of Interest

The authors declare no conflict of interest.